Influence of embedded cell on formation of broad acoustic band-gap in the three-component crystal slab*

HUA Jia, ZHANG Shu and CHENG Jianchun**

(State Key Laboratory of Modern Acoustics, Institute of Acoustics, Nanjing University, Nanjing 210093, China)

Received January 27, 2005; revised February 24, 2005

Abstract The influence of embedded cell on the formation of broad acoustic band-gap in the three-component crystal slab is analyzed by calculating the acoustic transmitted energy of the epoxy resin matrix with one embedded cell, which consists of the elastically soft rubber coat and the inner core steel cylinder. It is found that the broad band-gap in the three-component crystal slab results from localization of the acoustic wave energy in the rubber coat for a broad ultrasonic frequency interval. Comparison between experiments and calculations shows good agreement.

Keywords: acoustic band-gap, three-component system, embedded cell.

In the past two decades, the fact that acoustic crystals attenuate acoustic waves in some frequency domain have received a great deal of attention[1—6]. And much effort has focused on the theoretical and experimental researches of large band gaps in the acoustic band structure. Different geometries of two-dimensional composites, such as square[7,8], hexagonal[9,10], and boron nitride-like structure[11], have been investigated for prohibiting the transmission of acoustic waves in gaps. The design of board band-gaps has many engineering applications, such as acoustic transducers, acoustic filters, acoustic waveguide, etc. However, early work focused mainly on two-component systems, in which the acoustic band-gap is formed by the Bragg reflection. Recently, the three-component systems, which have the phenomenon of locally resonance, have been proposed by Liu et al.[12] and then have spurred a new area of research.

Recently, we reported the experimental and theoretical researches on the existence of broad acoustic band-gap in the three-component crystal slab[13]. This work is significant for design of board band-gaps in engineering applications. In order to clarify the physical mechanism of acoustic broad band-gap, in this paper, we calculate the spectra of the acoustic transmitted energy for the two- and three-component composites with single embedded cell, and analyze the influence of the embedded cell on formation of broad acoustic band-gap. It is found that the broad band-gap results from localization of the acoustic wave energy in the rubber coat for a broad ultrasonic frequency interval. Comparison between experiments and calculations shows good agreement.

1 Acoustic energy band: experiments

In experiments, we have manufactured two samples of the square arrays of steel cylinders inserted in an epoxy matrix with the same dimension of 90 mm × 60 mm × 50 mm. The lattice constant is $a = 7$ mm in all the samples. The steel cylinder has a diameter of $d_1 = 4$ mm in the two-component crystal slab. The diameter of steel cylinder with the rubber coating layer is $d_2 = 5$ mm (the thickness of rubber coating layer is 0.5 mm) and the core steel cylinder is $d_1 = 4$ mm. The sample contains 60 inclusions with 5 columns along the thickness direction (Fig. 1).

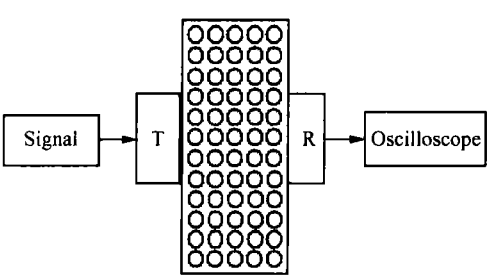

Fig. 1. Cross section of the experimental setup and sample.

* Supported by the National Fund for Distinguished Young Scholars (Grant No. 10125417) and the Major State Basic Research Development Program of China (Grant No. 51307)

** To whom correspondence should be addressed. E-mail: jccheng@nju.edu.cn

The experimental setup is based on the well-known ultrasonic transmission technique, which uses a couple of ultrasonic broadband transmitter/receiver transducers with a central frequency on the order of 1 MHz and a diameter of 25 mm (Panametrics, No. V102). The emitter is centered on the transversal face of the composite and the nearly parallel signal is perpendicular to the cylinders. A pulser/receiver generator (Panametrics, 5800PR) produces a short duration large amplitude pulse, which is applied to the transmitting transducer launching the probing longitudinal waves. The signal acquired by the receiver is digitized with a digital oscilloscope (Tektronix, TDS3032B) with the FFT capability to produce the power spectrum. Since it is difficult to measure the frequency response of the transducers, we recorded the reference spectrum from a pure epoxy sample almost with the same dimension and then normalized the detecting signal to guarantee that the power spectrum comes only from the sample.

Fig. 2 shows the spectra of acoustic transmitted energy of the two- and three-component crystal slabs, respectively. The former, in Fig. 2(a), exhibits a well-defined drop in intensity in the regions of 100—148 kHz and 325—415 kHz, where only the noise level is measured. However, a broad low transmission intensity appears clearly in the latter, as shown in Fig. 2(b), in which the gap extends from 220 kHz to 560 kHz followed by a sharp rise in transmission centered at 600 kHz. Apparently, this broad band-gap cannot be explained by the Bragg reflection so that the finite element method has been employed to verify the existence of broad band-gap in the three-component crystal slab[13].

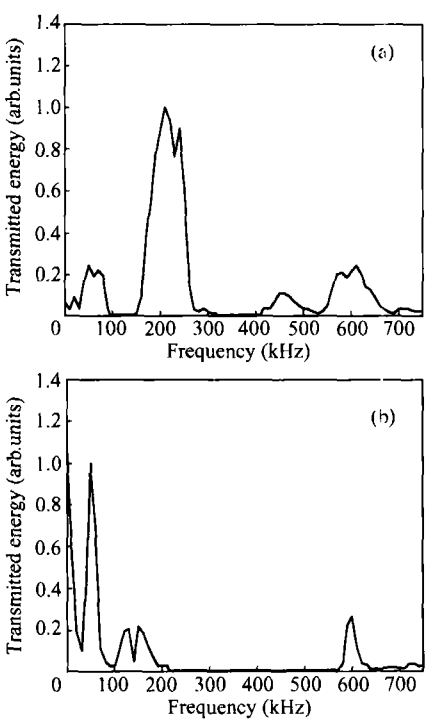

Fig. 2. Experimental transmitted energy spectra. (a) Two-component; (b) three-component phononic crystal slabs.

By comparing Fig. 2(a) and Fig. 2(b), we can see that the main difference between the two- and three-component crystal slabs is that there is an additional peak from 150 kHz to 300 kHz in the two-component sample. Because the material, the structure and the size of the steel cylinders are the same in the two samples, the disappearance of the peak in the three-component sample must owe to the rubber coating, so we focus on the effect of the rubber coating on acoustic band structure of the three-component crystal slab.

2 Localization of acoustic wave in rubber coating

We consider the composite with only one embedded cell in the epoxy resin matrix, and the matrix is supposed to be infinite in theoretical analysis. As shown in Fig. 3, the composite is divided into three regions: the matrix (I), the coating (II), and the core cylinder (III). The wave vector of the incident plane wave is parallel to the X-Z plane. Due to the error in the process of manufacturing samples, an angle α of the incident wave is introduced in the theoretical calculation. In a cylindrical coordinate system, the displacement vector $\boldsymbol{u}$ can be expressed in terms of potential functions ϕ, ψ and ξ[14]

$$\boldsymbol{u} = \nabla\phi + \nabla\times(\psi\boldsymbol{e}_z) + \nabla\times\nabla\times(\xi\boldsymbol{e}_z), \quad (1)$$

where $\boldsymbol{e}_z$ is a unit vector in the z direction. The incident plane longitudinal wave ϕ_0 of an angular frequency ω and of unit stress can be expanded as

$$\phi_0 = \frac{e^{ik_z z}}{\rho_0\omega^2}\sum_{n=-\infty}^{\infty} i^n J_n(k_{l1}' r)e^{in\theta}. \quad (2)$$

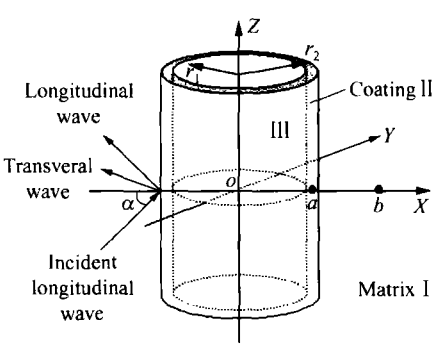

Fig. 3. The scattering of the incident longitudinal wave by one embedded cell (α is the incident angle).

Here, $J_n(x)$ is the n-order Bessel function; $k_{l1}' = k_{l1}\cos(\alpha)$, $k_z = k_{l1}\sin(\alpha)$, where k_{l1} is the longitudinal wave number. Obviously, k_{l1}' and k_z are the radial and axial vectors of the longitudinal wave, respectively. The time factor in ϕ_0 is dropped throughout for convenience.

Due to the interface, the longitudinal and transversal waves (S-V mode and S-H mode) in all the three materials can be excited by the incident plane longitudinal wave. And the potential functions ϕ_s, ψ_s and ξ_s of the waves in the matrix can be expanded as

$$\phi_s = e^{ik_z z}\sum_{n=-\infty}^{\infty} A_n H_n(k_{l1}' r)e^{in\theta},$$
$$\psi_s = e^{ik_z z}\sum_{n=-\infty}^{\infty} B_n H_n(k_{t1}' r)e^{in\theta},$$
$$\xi_s = \frac{e^{ik_z z}}{k_{t1}'}\sum_{n=-\infty}^{\infty} E_n H_n(k_{t1}' r)e^{in\theta}, \quad (3)$$

where $H_n(x)$ are the n-order Hankel functions of the first kind. Based on the Snell's law, the axial wave vectors of the scattered longitudinal wave, the scattered transversal wave and the incident wave are the same, such as k_z. The radial vector of the scattered transversal wave is $k_{t1}'^2 = k_{t1}^2 - k_z^2$, where k_{t1} is the transversal wave number in the matrix. The potential functions ϕ_1, ψ_1 and ξ_1 in the matrix can be expressed as the summations of the incident and scattered wave:

$$\phi_1 = \phi_0 + \phi_s,$$
$$\psi_1 = \psi_s,$$
$$\xi_1 = \xi_s. \quad (4)$$

The potential functions of the excited waves in regions II and III can be expanded as

$$\phi_2 = e^{ik_z z}\sum_{n=-\infty}^{\infty}[P_n J_n(k_{l2}' r) + Q_n N_n(k_{l2}' r)]e^{in\theta},$$
$$\psi_2 = e^{ik_z z}\sum_{n=-\infty}^{\infty}[R_n J_n(k_{t2}' r) + S_n N_n(k_{t2}' r)]e^{in\theta},$$
$$\xi_2 = \frac{e^{ik_z z}}{k_{t2}'}\sum_{n=-\infty}^{\infty}[U_n J_n(k_{t2}' r) + V_n N_n(k_{t2}' r)]e^{in\theta}, \quad (5)$$

where $N_n(x)$ are the n-order Neumann functions, k_{l2}' and k_{t2}' are the radial vectors of the longitudinal and transversal waves of region II, respectively, and

$$\phi_3 = e^{ik_z z}\sum_{n=-\infty}^{\infty} C_n J_n(k_{l3}' r)e^{in\theta},$$
$$\psi_3 = e^{ik_z z}\sum_{n=-\infty}^{\infty} D_n J_n(k_{t3}' r)e^{in\theta},$$
$$\xi_3 = \frac{e^{ik_z z}}{k_{t3}'}\sum_{n=-\infty}^{\infty} F_n J_n(k_{t3}' r)e^{in\theta}, \quad (6)$$

where k_{l3}' and k_{t3}' are the radial vectors of the longitudinal and transversal waves of region III, respectively. The axial wave vectors in regions II and III are both k_z.

A linear algebraic system with the unknown coefficients in Eqs. (3), (5) and (6) will be obtained by using the continuity conditions of displacement and stress at $r = r_1$ and $r = r_2$. With these twelve coefficients, one can obtain the displacement potential functions of acoustic waves in all three materials. In the same method, the displacement potential functions in two-component composite without the rubber coating can also be calculated.

According to sizes of the embedded cell in the experiments (the diameter of steel cylinder is 4 mm and the thickness of the rubber coating is 0.5 mm), the spectra of acoustic transmitted energy at point a (inside the rubber coating layer) and point b (inside the epoxy resin matrix) are calculated numerically for the two-component (the steel cylinder with a rubber coating) embedded cell, and only point b must be considered for the one-component (the steel cylinder without a rubber coating) embedded cell, as shown in Fig.4(a), Fig. 5(a) and Fig. 5(b), respectively. Correspondingly, two samples of the two- or three-component composite are manufactured, which are made up of the epoxy resin matrix embedded only one steel cylinder with and without a rubber coating, respectively. The spectra of acoustic transmitted energy at point b are measured experimentally, as shown in Fig.4(b) and Fig.5(c), respectively.

The calculation shows that the amplitude of the acoustic waves from 150 kHz to 300 kHz in the rubber coating is much greater than other frequency region by about 1—2 order of magnitude, as shown in Fig.5(a). Correspondingly, in Fig. 5(b), the low transmitted spectrum appears in the same frequency range in the epoxy resin matrix. The energy of acoustic waves in the range of 150 kHz to 300 kHz has been localized in the rubber coating and forbidden to transmit into the epoxy resin matrix. It is the result of the local resonance in the rubber coating.

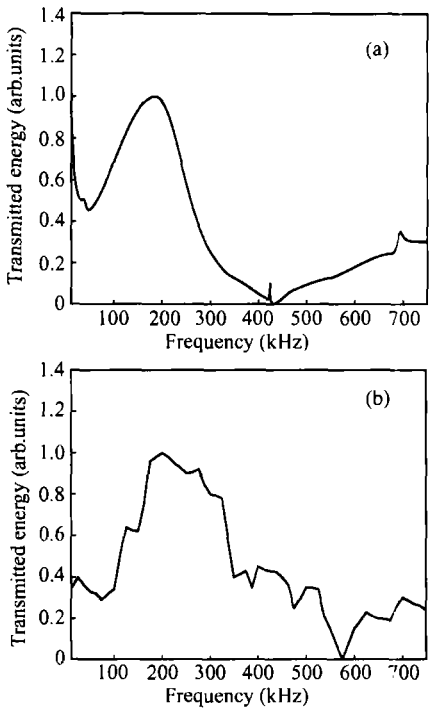

Fig. 4. Transmitted energy spectra of two-component composite at point b ($r = 0.004$ m). (a) Theoretical result; (b) experimental result.

Comparing Fig. 4(a) with Fig. 5(b), the region with the low transmitted energy from 150 kHz to 300 kHz in the matrix of three-component composite does not exist in the spectrum of two-component composite. This difference can explain the broad band-gap of the spectrum of acoustic transmitted energy for the three-component crystal slab very well in Fig. 2(b). Because of the localization of the acoustic wave in the rubber coating, the peak in the range from 150 kHz to 325 kHz in the spectrum of two-component crystal slab is attenuated to noise level.

The discrepancy between the theoretical and experimental curves in Fig. 4(b) and Fig. 5(c) maybe result from two main factors: (1) the matrix is considered as infinite in the theoretical calculation, but it is finite in the experiment; (2) the acoustic energy is calculated at a geometric point b in the theory, but the size of the transducer is finite in the experiment.

After the spectra of acoustic transmitted energy are analyzed for only one embedded cell, the spatial distributions of the acoustic field with different frequencies are calculated numerically in a three-component crystal slab. According to Fig. 2 and Fig. 5(a), two typical frequencies, 220 kHz and 600 kHz, are chosen, and the former is in the region of the rubber coating localization and in the acoustic band-gap. Fig. 6(a) and Fig. 6(b) show the amplitude output (the Z axis) of the longitudinal displacement field u_x in the three-component crystal slab at frequency of

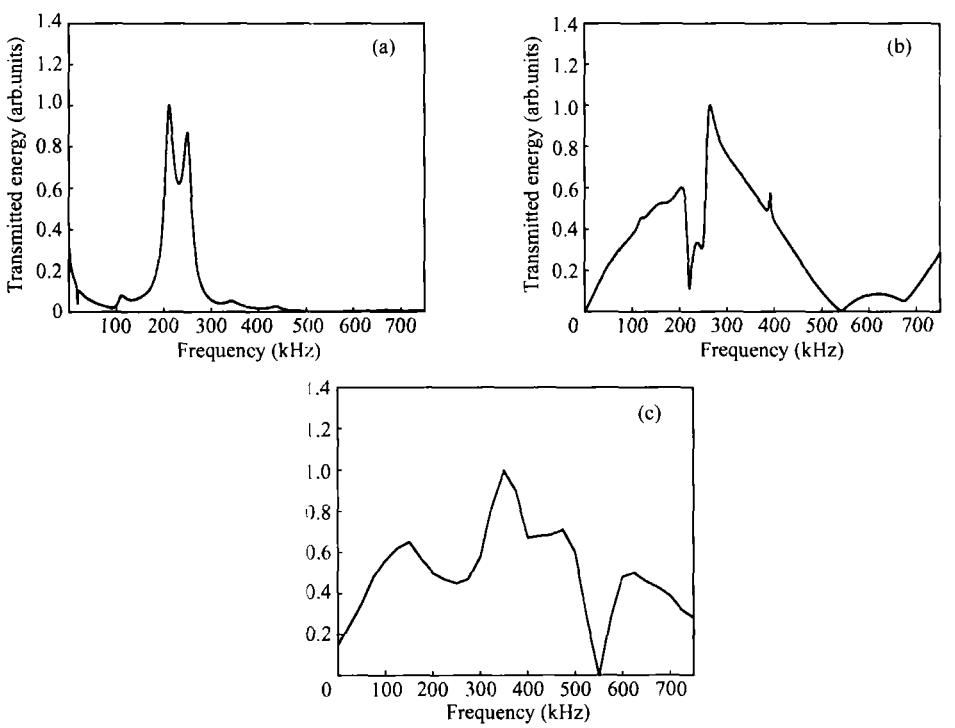

Fig. 5. Transmitted energy spectra of three-component composite. (a) Theoretical result, at point a ($r = 0.00225$ m); (b) theoretical result, at point b ($r = 0.004$ m); (c) experimental result, at point b ($r = 0.004$ m).

220 kHz and 600 kHz, respectively. We can see from the figures that the displacement of acoustic waves in the rubber coating is much greater than other materials. The large displacement in the rubber coating results from its softness and low elastic constants. In Fig. 6(a), the wave amplitude in rubber at 220 kHz is about 140 times larger than that at 600 kHz in Fig. 6 (b), which can verify the existence of the local resonance in rubber coating again.

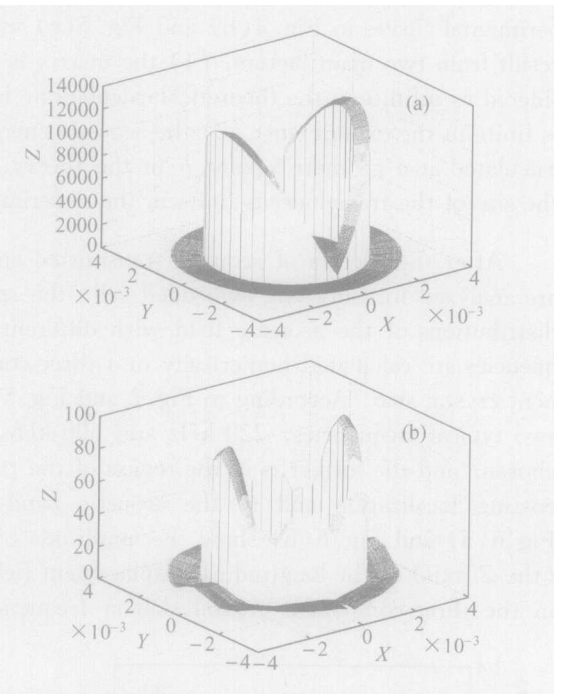

Fig. 6. The amplitude of longitudinal displacement field u_x in the three-component crystal slab at frequency of (a) 220 kHz and (b) 600 kHz. The direction of the incident wave is the X direction.

3 Conclusion

In summary, we have calculated the spectra of the acoustic transmitted energy for the two- and three-component composites with single embedded cell and the spatial distributions of the displacement field u_x in the three-component crystal slab. It is proved unambiguously that the broad acoustic band-gap in the three-component crystal slab comes from the local resonance of acoustic wave in the rubber coating. The elastically soft materials such as rubber can broaden the width of the band-gap. And in light of the agreement between the measured and calculated results, we believe that this method of broadening the gaps will be highly practical.

References

1 Sigalas M. M. and Economou E. N. Band structure of elastic waves in two dimensional system. Solid State Commun., 1993, 86: 141—143.
2 Kushwaha M. S., Halevi P., Martinez, G. et al. Theory of acoustic band structure of periodic elastic composite. Phys. Rev. B, 1994, 49: 2313—2322.
3 Montero de Espinosa F. R., Jiménez E. and Torres M. Ultrasonic band gap in a periodic two-dimensional composite. Phys. Rev. Lett., 1998, 80: 1208—1211.
4 Torres M., Montero de Espinosa F. R., Garcia-Pablos D. et al. Sonic band gaps in finite elastic media: Surface states and localization phenomenon in linear and point defects. Phys. Rev. Lett., 1999, 82: 3054—3057.
5 García-Pablos D., Sigalas M., Montero de Espinosa F. R. et al. Theory and experiments on elastic band gaps. Phys. Rev. Lett., 2000, 84: 4349—4352.
6 Mártinez-Sala R., Sancho J., Sanchez J. V. et al. Sound attenuation by sculpture. Nature, 1995, 378: 241—241.
7 Vasseur J. O., Djafari-Rouhani B., Dobrzynski L. et al. Complete acoustic band gaps in periodic fibre reinforced composite materials: The carbon/epoxy composite and some metallic system. J. Phys. Condens. Matter, 1994, 6: 8759—8770.
8 Kushwaha M. S., Halevi P., Dobrzynski L. et al. Acoustic band structure of periodic elastic composite. Phys. Rev. Lett., 1993, 71: 2022—2025.
9 Sigalas M. M. and Economou E. N. Elastic waves in plates with periodically placed inclusion. J. Appl. Phys., 1994, 75: 2845—2850.
10 Kushwaha M. S. and Halevi P. Band-gap engineering in periodic elastic composite. Appl. Phys. Lett., 1994, 64: 1085—1087.
11 Vasseur J. O., Djafari-Rouhani B., Dobrzynski L. et al. Acoustic band gaps in fibre composite materials of boron-nitride structure. J. Phys. Condens. Matter, 1997, 9: 7327—734.
12 Liu Z., Zhang X., Mao Y. et al. Locally resonant sonic materials. Science, 2000, 289: 1734—1736.
13 Zhang S. and Cheng J. C. Existence of broad acoustic band gaps in three-component composite. Phys. Rev. B, 2003, 68: 245101—245106.
14 White R. M. Elastic wave scattering at a cylindrical discontinuity in a solid. J. Acoust. Soc. Am., 1958, 30: 771—785.